9th Liege Conference : Materials for Advanced Power Engineering 2010
edited by J. Lecomte-Beckers, Q. Contrepois, T. Beck and B. Kuhn.

IMPROVED CREEP AND OXIDATION BEHAVIOR OF A MARTENSITIC 9CR STEEL BY THE CONTROLLED ADDITION OF BORON AND NITROGEN

Peter Mayr[1,2], Ivan Holzer[2], Francisca Mendez-Martin[2], Mihaela Albu[3], Stefan Mitsche[3], Vanessa González[4], Alina Agüero[4]

[1] Department of Materials Science and Engineering, Massachusetts Institute of Technology, 77 Massachusetts Av, MA 02139, USA

[2] Institute of Materials Science and Welding, Graz University of Technology, Kopernikusgasse 24, 8010 Graz, Austria

[3] Institute for Electron Microscopy, Graz University of Technology, Steyrergasse 17, A-8010 Graz, Austria

[4] Instituto Nacional de Técnica Aeroespacial, Ctra. de Ajalvir Km 4, 28850 Torrejón de Ardoz, Spain

Abstract

This manuscript gives an overview on recent developments of a martensitic steel grade based on 9Cr3W3CoVNb with controlled additions of boron and nitrogen. Alloy design by thermodynamic equilibrium calculations and calculation of boron-nitrogen solubility is discussed. Out of this alloy design process, two melts of a 9Cr3W3CoVNbBN steel were produced. The investigation focused on microstructural evolution during high temperature exposure, creep properties and oxidation resistance in steam at 650°C.
Microstructural characterization of "as-received" and creep exposed material was carried out using conventional optical as well as advanced electron microscopic methods. Creep data at 650°C was obtained at various stress levels. Longest-running specimens have reached more than 20,000 hours of testing time. In parallel, long-term oxidation resistance has been studied at 650°C in steam atmosphere up to 5,000 hours.
Preliminary results of the extensive testing program on a 9Cr3W3CoVNbBN steel show significant improvement in respect to creep strength and oxidation resistance compared to the state-of-the-art 9 wt. % Cr martensitic steel grades. Up to current testing times, the creep strength is significantly beyond the +20% scatterband of standard grade P92 material. Despite the chromium content of 9 wt. % the material exhibits excellent oxidation resistance. Steam exposed plain base material shows comparable oxidation behavior to coated material, and the corrosion rate of the boron-nitrogen controlled steel is much lower compared to standard 9 wt.% Cr steel grades, P91 and P92.

Keywords: 9-12% chromium steels, microstructural evolution, creep testing, oxidation testing

1. Introduction

In Japan and Europe, research and development works in the field of advanced martensitic creep resistant steels has a long history [1-3]. The applications for such materials are in particular large diameter and thick section boiler components, such as main steam pipes and headers of ultra-supercritically (USC) operated power plants. The current target of ferritic steel development is set to a creep rupture strength of 100 MPa after 100,000 hours at 650°C and oxidation rates lower than for grade P91 steel.

Within the last years, the alloy design philosophy for martensitic steels strongly targets the enhancement of long-term microstructural stability [4]. Migration of lath and block boundaries, causing the coarsening of martensite laths and blocks by annihilation of excess dislocations, closely correlates with the onset of accelerated creep. A fine dispersion of $M_{23}C_6$ and MX particles, which exert a pinning force on migrating boundaries and dislocations, has been identified as main contributor in suppressing recovery of the martensitic microstructure.
The work presented in this manuscript is following an extensive research program published by the National Institute for Materials Science (NIMS), Japan [4]. In detail, the NIMS alloy design concept follows stabilization of $M_{23}C_6$ carbides and grain boundaries by the addition of boron in combination with finely dispersed MX particles as a possible solution to stabilize the martensitic substructure. As basis for the systematically study of the influence of boron and nitrogen on long-term creep behavior, a Fe-0.08C-9Cr-3W-3Co-0.2V-0.05Nb (wt. %) steel with different concentrations of boron and nitrogen was investigated [5,6].

The influence of boron on 9Cr3W3CoVNb steel was studied in the range of 0 to 140 ppm (parts per million) while nitrogen level was kept constant at a minimum between 10 to 30 ppm [5]. The influence of boron additions on creep properties was studied by uniaxial-creep testing at 650°C at different stress levels. At stress levels higher than 100 MPa, no big difference in creep strength between 0B, 0.0048B and 0.0092B steel was found. Only 0.0139B steel showed improved creep strength. While at lower stress levels, creep strength of the lower boron steels decreased significantly, 0.0139B steel showed a stable creep behavior. It was concluded that controlled addition of boron can delay the drop of creep strength in 9Cr3W3CoVNb steel. As a result of the boron series creep tests, a boron content of 140 ppm was identified as optimum for improved creep behavior.
The combined effect of boron plus additional MX precipitation was studied by 9Cr3W3CoVNb test melts with a fixed boron content of 140 ppm and varying nitrogen levels of 15, 79 and 650 ppm [6]. Increasing the nitrogen level to 79 ppm resulted in further improvement of the creep strength of the base 9Cr3W3CoVNb-0.0140B steel. However, further increase of nitrogen to 650 ppm showed no beneficial effects and in turn reduced creep strength of the alloy.
The main idea behind the NIMS alloying concept is to combine boron-strengthening with nitride-strengthening. However, excess addition of nitrogen in combination with boron causes the formation of boron nitrides (BN) during processing and heat treatments at elevated temperatures. Precipitation of boron nitrides offsets the beneficial effect of boron and nitrogen addition. Sakuraya et. al [7] showed in their work on BN formation in high Cr heat resistant steels that, a particular relationship between boron and nitrogen has to be kept to avoid

formation of coarse BN particles. From their experimental observations the authors derived a mathematic formulation of the solubility product of BN.

Within the present work, the NIMS alloy design strategy is expanded by thermodynamic studies of the boron nitride solubility product. Slightly modified alloy chemistry is proposed and first results of creep and oxidation tests as well as the microstructural evolution during creep are presented.

1. Experimental

1.1. Alloy Design

Thermodynamic equilibrium calculations were performed using the software Matcalc [8-11] utilizing the thermodynamic database Fe-data6 [12]. The description of BN in the database was slightly modified, based on the work of Fountain et al. [13]. Alloy design was supported through a calculated equilibrium phase diagram for the 9Cr3W3CoVNbBN steel and a boron nitride and boride solubility diagram.

1.2. Materials

A 20 kg heat (Heat 1) of 9Cr3W3CoVNb steel with controlled additions of 120 ppm boron and 130 ppm nitrogen was produced by vacuum induction melting. The addition of boron and nitrogen was set to avoid the formation of large boron nitrides but still allow the precipitation of strengthening MX particles. For homogenization of Heat 1, the ingot (110 mm square) was forged to final dimensions of 50 mm square. A second heat (Heat 2) of a 9Cr3W3CoVNb steel with slightly reduced boron (110 ppm) and nitrogen (100 ppm) content was cast (100 kg) and rolled to 20 mm thick plates. The exact chemical composition in weight % (wt. %) for Heat 1 and Heat 2 is given in Table 1. The final quality heat treatment for both heats consisted of normalizing at 1150 °C for 1 hour followed by tempering at 770 °C for 4 hours.

Table 1: Chemical composition of 9Cr3W3CoVNbBN test melts in wt. % (balanced Fe).

Analysis	C	Si	Mn	Cr	W	Co	V	Nb	B	N
Heat 1	0.074	0.29	0.44	9.26	2.84	2.95	0.21	0.056	0.012	0.013
Heat 2	0.090	0.30	0.51	9.26	2.92	2.88	0.20	0.050	0.011	0.010

In both heats, precipitation of BN particles was investigated. Material of Heat 1 was used for microstructural characterization and creep testing. Fractured creep samples were investigated by means of optical and electron microscopy to determine the microstructural evolution during creep. Heat 1 material was also used for oxidation testing in steam atmosphere.
Heat 2 material was used for basic metallographic investigations and for additional creep tests.

1.3. Steam Oxidation Laboratory Testing

The schematic of the closed loop laboratory rig employed at INTA is shown in *Figure 1*. Prior to testing, laboratory air is displaced from the chamber by means of N_2 which is kept flowing while heating up to the test temperature (approximately 600°C/h). Once the test

temperature is reached, the N_2 flow is closed and pure steam is introduced at a linear velocity of 8 cm/s. To carry out weight measurements or to remove samples, the furnace is cooled to about 300°C under N_2 atmosphere and the specimens are subsequently removed. The reheat cycle is also carried out under N_2 atmosphere.

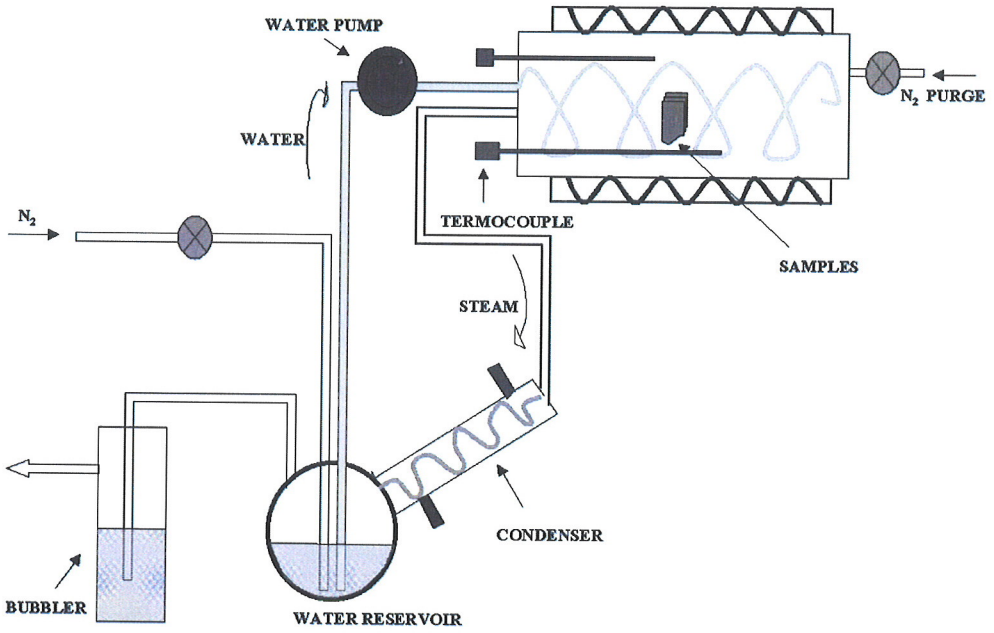


Figure 1: Sketch of the closed loop laboratory test rig for the oxidation testing of samples in steam atmosphere at 650°C.

1.4. Microstructure Characterization

Base material microstructure was characterized by light optical microscopy, scanning electron microscopy (SEM) and analytical transmission electron microscopy (TEM). Precipitation of BN was studied by SEM and energy dispersive X-ray spectroscopy (EDS) on fracture surfaces of base material specimens. The smallest BN particle size being able to identify is about 0.3 µm. Details are reported in [14]. The oxidized specimens were characterized by optical and field emission scanning electron microscopy (FESEM) using a JEOL JSM 840 system equipped with an energy dispersive X-ray spectrometer (EDS) KEVEX MICROANALYST 8000 with a RÖNTEC signal processor.

2. Modified Alloy Design Concept

The investigated alloys are based on a 9Cr3W3CoVNbBN steel. The calculated equilibrium phase diagram for the chemical composition equal to that of Heat 1 (see Table 1) indicates that the steel should be free of delta ferrite at room temperature. The nominal chromium content of 9 wt.% enables a complete austenitization on cooling in the temperature range from 1183°C to 881°C. Normalizing at 1150°C will therefore dissolve most of the precipitates

formed during solidification and allow a homogenization of the elemental distribution through diffusion. On cooling, a uniform martensitic microstructure will form which then is tempered at 770°C.

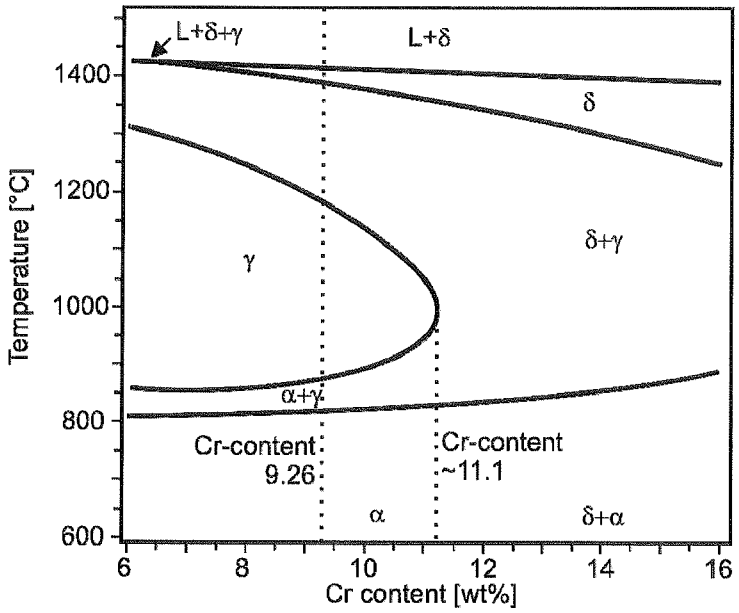


Figure 2: Calculated equilibrium phase diagram with varying chromium content for a 9Cr3W3CoVNbBN steel with a chemical composition equal to that of Heat 1.

To take advantage of boron and nitrogen addition, the formation of large boron nitrides (BN) and borides (M_2B) has to be avoided. Therefore, in the present work the allowable boron and nitrogen limits for high chromium martensitic steels were determined by thermodynamic equilibrium calculations. The BN solubility product for a 9Cr3W3CoVNbBN steel, based on the chemical composition of Heat 1, was calculated for various B/N ratios and different normalizing temperatures, including also possible formation of borides (M_2B). Similar to boron nitrides, boride particles would also reduce the amount of boron dissolved in the metal matrix or incorporated in chromium carbides ($M_{23}C_6$) and therefore diminish the beneficial effect of boron addition.

Results of the BN solubility calculation are shown in *Figure 3*. The solubility products (solid lines) are shown for different normalizing temperatures ranging from 900°C to 1250°C. The dashed grey lines represent the solubility product for the M_2B phase. For reason of comparison, the BN solubility lines reported by Fountain et al. [13] at 1150°C and Sakuraya et al. [15] are included in the figure.

The grey shaded area in *Figure 3* indicates critical B/N ratios e.g. at 1250°C where BN formation is to be expected. No formation of BN is expected below the respective BN solubility line.

Figure 3 clearly shows that the experimental findings reported by Sakuraya et al. [15] are well described by the thermodynamic equilibrium considerations in the temperature range between 900°C and 1250°C. Sakuraya et al. [7] reported no BN formation for temperatures higher than 1250°C.

Due to the temperature dependence of the BN solubility product it can be assumed that coarse BN (>1μm) exist for high boron and nitrogen contents and low normalizing temperatures.

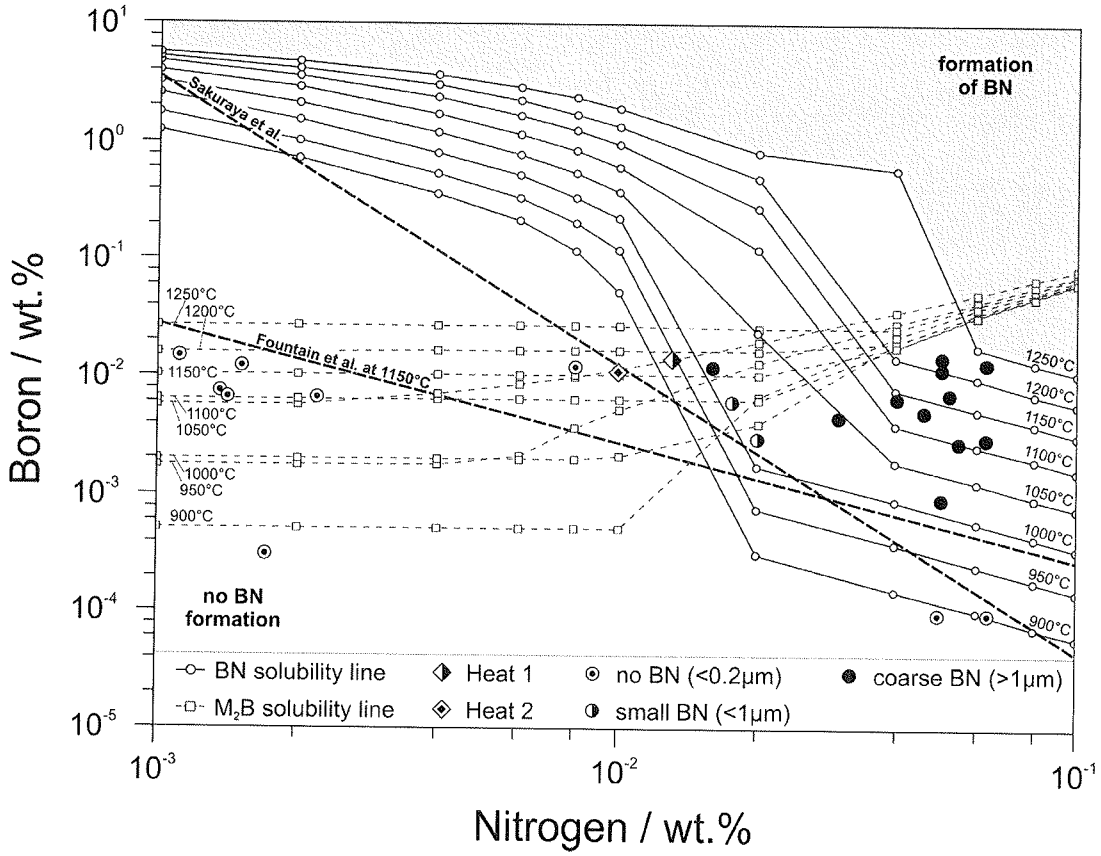


Figure 3: BN solubility product for a 9Cr3W3CoVNbBN steel as a function of normalizing temperature in the range of 900°C to 1250°C. The grey shaded areas indicate BN formation. The calculation is compared to the solubility products reported by Sakuraya et al. [15], and Fountain et al. [13], and the two heats investigated within this work.

3. Microstructure of 9Cr3W3CoVNbBN steel

Optical micrographs of 9Cr3W3CoVNbBN base material (Heat 1) show a tempered martensitic microstructure (see *Figure 4*). The average prior austenite grain size is 250 µm in diameter, and precipitates are finely distributed mainly along prior austenite grain and martensite lath boundaries.

Via electron microscopy, MX (V,Nb)(N,C) carbonitrides and $M_{23}C_6$ $(Cr,Fe,Mo,W)_{23}C_6$ carbides have been identified at grain and lath boundaries and/or in the matrix of the base material. MX (V,Nb)(N,C) particles have a representative diameter smaller than 100 nm, and Cr-rich carbides have a diameter between 150 and 250 nm. By SEM and EDS only very few and small (<1µm) BN particles for Heat 1 and no BN particles for Heat 2 have been detected. A detailed description of the method of detecting BN particles is given in [15]. These experimental findings support the results of the thermodynamic equilibrium calculations in the alloy design stage.

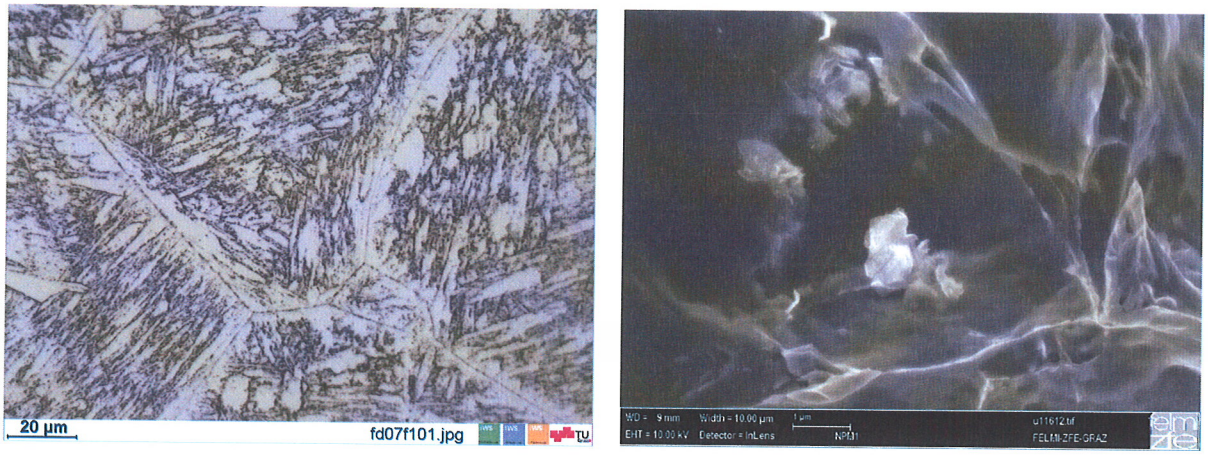


Figure 4: Optical micrograph of normalized and tempered 9Cr3W3CoVNbBN base material (left) and small BN particle (right) identified by EDS - both images for Heat 1.

After creep exposure for 8,971 hours at 650 °C and 130 MPa, light-optical and electron-microscopic investigations have been performed to study the microstructural evolution during creep exposure. The prior austenite grain and martensite lath structure, after almost 10,000 h of creep, show no significant changes. The precipitate size and number density of carbonitrides and carbides remain almost the same as in the base material. The electron microscopy investigation reveals the precipitation of two new phases: laves phase (intermetallic phase A_2B, $(Fe,Cr)_2(W,Mo)$ with approximately 38 atom % of tungsten and more than 45 atom % of iron, distributed mainly at the grain boundaries, and modified Z-phase (complex nitride [(Cr,V,Nb)N]) with a very low phase fraction. Details on the microstructural evolution of 9Cr3W3CoVNbBN steel during creep exposure can be found in [16]. Based on this study, an enhanced microstructural stability can be attributed to 9Cr3W3CoVNbBN steel.

4. Oxidation behavior

Specimens of 9Cr3W3CoVNbBN (Heat 1) were exposed to pure, flowing steam at 650°C for 4,908 h. *Figure 5* shows the mass variation of the new steel as function of time as well as that of 9 wt.% ferritic steels P91 and P92 for comparison purposes. 9Cr3W3CoVNbBN exhibits a mass gain considerably lower than that of the other two 9 wt. % Cr steels. This behavior is surprising, as work done by several research groups have indicated the steam oxidation resistance of steels strongly correlates with the Cr contents, and results so far have indicated that 9 wt. % Cr steels oxidized very fast when exposed to steam at T > 600°C [17-20]. For instance, Quadakkers and collaborators have concluded that a chromium content of 11 wt. % or more is required to form a protective scale [17].

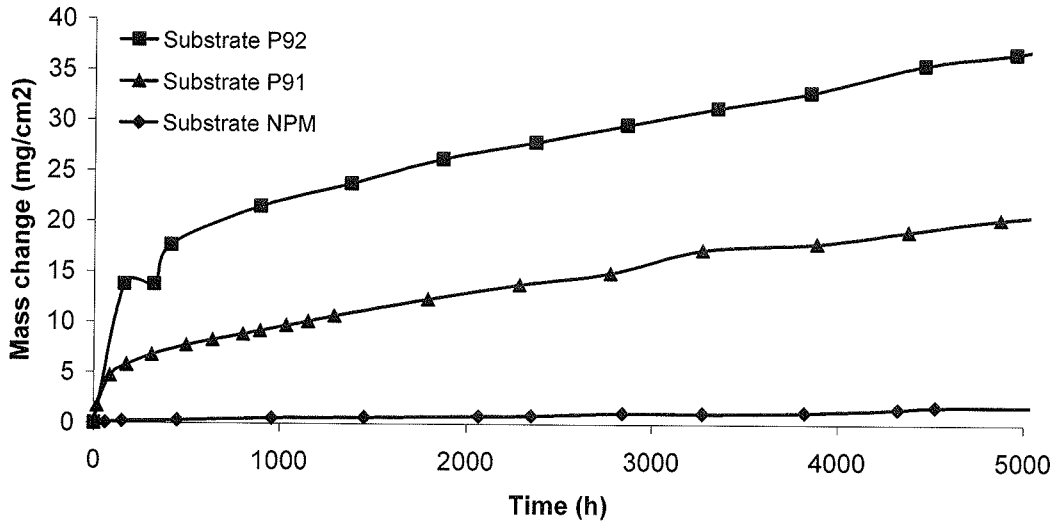


Figure 5: Mass gain of conventional (P91, P92) 9 wt. % steel and 9Cr3W3CoVNbBN (NPM1) substrates exposed to flowing steam (1 bar) at 650° C

Figure 6 shows an image of a specimen exposed to 650°C hot steam for 4,908 h. Several nodular features can be observed, especially at the samples edges but most of the surface still appears to be smooth. On the cross section of the exposed surface, a very thin (< 100 nm) Cr and O rich layer, most likely Cr_2O_3 can be observed with difficulty. This type of oxide is typical of steels containing 11 wt. % of Cr or more. Quadakkers found that Co tends to increase the oxidation resistance of 9-12 Cr wt. % ferritic steels [17], but not to the extent observed for 9Cr3W3CoVNbBN. On the other hand, other groups have observed that the higher the W content, the lower the oxidation resistance of these types of steels [18,21,22]. It is therefore not clear yet why this 9 wt. % steel forms a protective oxide layer and exhibits such high steam oxidation resistance. Further studies are required.

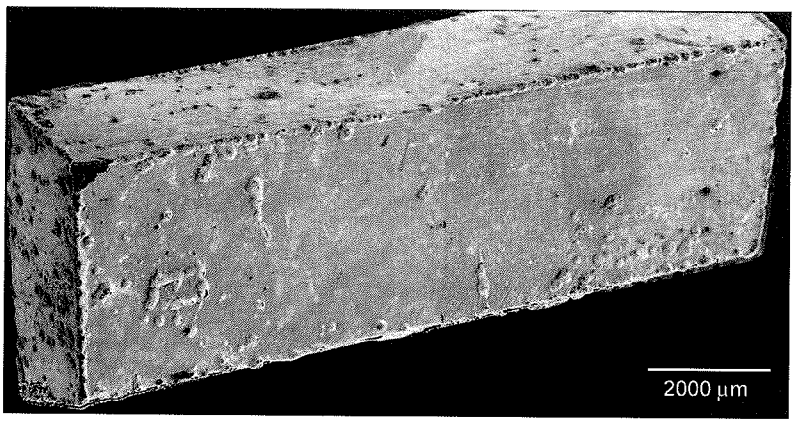


Figure 6: SEM image of a 9Cr3W3CoVNbBN specimen exposed to steam at 650°C for 4,908 h

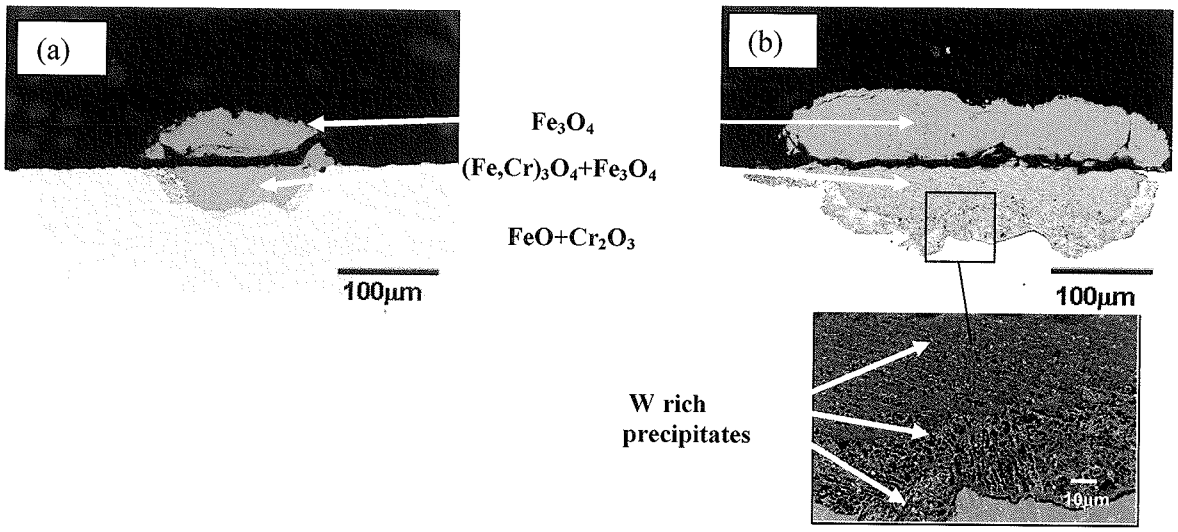


Figure 7: FESEM image of the cross section of 9Cr3W3CoVNbBN exposed to steam at 650°C at a nodule site: (a) for 1,260 h, (b) for 4,908 h

The cross section of representative nodules formed after 1,260 and 4,908 h are shown in *Figure 7a* and *b* respectively. The microstructure corresponds to a dual oxide layer similar to that observed on ferritic steels containing 9 wt.% in Cr, with a top outwards growth of a Fe_3O_4 layer and an inside growing mixed oxide layer containing (Fe, $Cr)_3O_4$, FeO and Cr_2O_3 [23] which also contains W, Co and V. Interestingly, W rich nanoscale precipitates which are also present in the substrate can be observed in this inner oxide layer. The nodules in the 1,260 h specimen exhibit lower thickness and width than those observed in the specimen exposed for 4,908 h, indicating that these oxides are growing and therefore are not protective. Moreover, the number of nodules on the 4,908 h specimen is higher than that observed on the 1,260 h specimen.

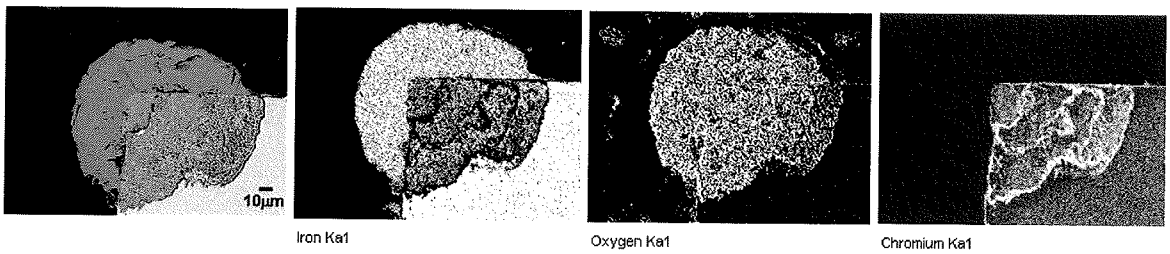


Figure 8: Cross section of the edge of a 9Cr3W3CoVNbBN specimen exposed to steam at 650° C for 4,908 h

At one specimen's edge (*Figure 8*), the corresponding EDS composition map reveals Cr-rich layers within the inner oxide and the original specimen surfaces. The average Cr content (19 wt. %) in this inner oxide zone is significantly higher than that of the substrate, but because it is not uniformly distributed it is not of a protective nature. According to Quaddakers and coworkers, this pattern results from the repetition of cycles in which Cr rich spinels form due to rapid Cr diffusion from the bulk alloy until the spinel cannot be sustained due to continuous

Cr depletion, resulting in the formation of Fe rich oxides [17]. Formation of oxidation nodules has been observed on oxidation resistant 12 wt. % steels and has been attributed to compositional inhomogeneity [17,24]. For this 9Cr steel the presence of nodules can be rather attributed to local cracks, imperfections and/or rupture of the protective scale on a Cr depleted substrate. The fact that the samples edges are fully covered with nodules support this hypothesis as due the higher triaxiality of stresses, corners and edges are more prone to develop cracks.

5. Creep Strength

Uniaxial creep tests of 9Cr3W3CoVNbBN base material specimens have been carried out at 650°C. Both Heat 1 specimens tested at 130 MPa and 100 MPa have already fractured, as shown in *Figure 9*. The base material specimen tested at a higher stress level of 130 MPa fractured after 8,971 h. This corresponds to an improvement of rupture stress at approximately 9,000 hours of +60 MPa and +40 MPa compared to grades P91 and P92 respectively. After 23,997 hours of creep exposure, creep rupture strength of 9Cr3W3CoVNbBN steel is still beyond the +20% average creep strength of grade 92 material. Heat 2 material tests are still running but up to almost 10,000 hours of testing, creep strength is superior to that of standard grade 92 material by more than +20%.

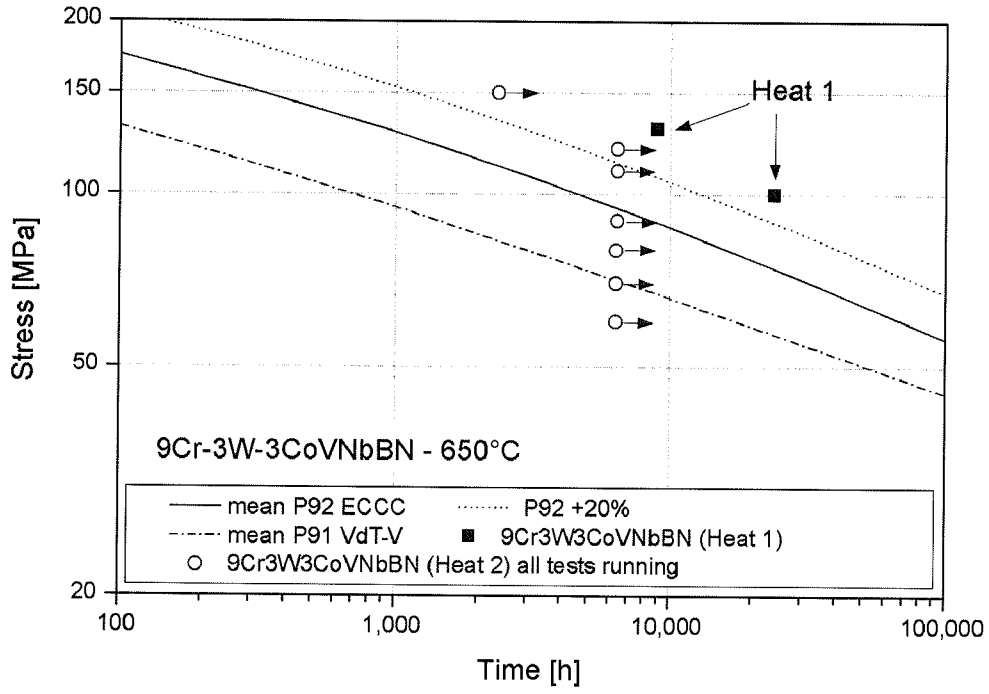


Figure 9: Creep testing data of 9Cr3W3CoVNbBN base material of Heat 1 and Heat 2 at 650°C compared to creep rupture data of well-established grades P91 and P92.

6. Summary and Conclusions

Alloy design for a 9 wt. % Cr steel has been successfully improved by thermodynamic studies of the boron-nitrogen solubility product. The boron and nitrogen content of a 9Cr3W3CoVNbBN steel was adjusted to have either only very small boron nitrides (Heat 1) or no precipitation of BN (Heat 2). This confirms that in these two heats most of the boron stays either in solution or is incorporated in $M_{23}C_6$ carbides. Therefore, the added boron can develop its maximum strengthening contribution.

The boron strengthened 9Cr3W3CoVNbBN steels exhibits an unexpected high resistance to steam oxidation at 650°C. Despite its low Cr content it develops a thin Cr rich protective oxide scale. However, several oxidation nodules form, very likely due to imperfections in the protective oxide layer. These nodules grow in thickness, width and number as a function of steam exposure time. Nevertheless, the increased oxidation resistance of the new steels shows high potential and is currently studied in detail.

The creep behavior up to testing times of almost 25,000 hours at 650°C is very promising. The 9Cr3W3CoVNbBN steel shows an improved creep rupture strength more than +20% beyond the average creep strength of standard grade 92 steel. This higher creep rupture strength is attributed to an enhanced microstructural stability due to the controlled addition of boron and nitrogen. Soluble boron stabilizes the martensitic microstructure and delays recovery whereas boron incorporated in $M_{23}(C,B)_6$ carbides reduces their tendency to coarsening.

Acknowledgements

PM would like to thank the Austrian Academy of Sciences and the Max Kade Foundation for granting a one-year research fellowship. The authors would like to acknowledge the support by the European Cooperation in Science and Technology (COST) through Action 536 "Alloy development for Critical Components of Environmental friendly Power planT (ACCEPT)" and the Austrian Research Promotion Agency - FFG (#818512). AA and VG wish to acknowledge the Spanish Ministry of Science and Innovation for the financial support (ENE2008-06755-C02-01).

References

[1] Kern T U, Wieghardt K and Kirchner H, in 4th int conf Advances in Materials Technology for Fossil Power Plants, Hilton Head Island, ASM International, 2005.
[2] Masuyama F, in 4th int conf Advances in Materials Technology for Fossil Power Plants, Hilton Head Island, ASM International, 2005.
[3] Cerjak, H.-H.; Dimmler, G.; Holzer, I.; Kozeschnik, E.; Mayr, P.; Pein, C.; Sonderegger, B.: Materials science forum 539-543 (2007) , S. 2954 - 2959
[4] Abe F, in 4th int conf Advances in Materials Technology for Fossil Power Plants, Hilton Head Island, SC, EPRI, 2004.
[5] Abe F, Horiuchi T and Sawada K, Materials Science Forum, 2003, 426-432, 1393-1398.
[6] Semba H and Abe F, "in 4th int conf Advances in Materials Technology for Fossil Power Plants, Hilton Head Island, SC, EPRI, 2004.

[7]Sakuraya K., Okada H., Abe F., ISIJ Int., vol. 46 (2006), 1712.
[8]Kozeschnik E., Buchmayr B., Mathematical Modelling of Weld Phenomena 5, Institute of Materials, London, 2001, 349.
[9]Svoboda J., Fischer F. D., Fratzl P., Kozeschnik E., Mater. Sci. Eng. A, vol 385 (2004) 166.
[10]Kozeschnik E., Svoboda J., Fratzl P., Fischer F. D., Mater. Sci. Eng. A, vol 385 (2004) 157.
[11]Kozeschnik E., Svoboda J., Fischer F. D., CALPHAD, vol 28 (2005) 379.
[12]Saunders M., Fe-data6.tdb.
[13] R.W. Fountain, Chipman J., Transactions of the Metallurgical Society of AIME, vol. 224 (1962) 599.
[14]Mayr P., PhD-Thesis, Graz University of Technology, 2007
[15]Sakuraya K., Okada H., Abe F., in: Advances in Materials Technology for Fossil Power Plants: Proceedings of the Fourth International Conference, (2004) 1270.
[16] Mayr, P.; Mendez Martin, F.; Albu, M.; Cerjak, H.-H.: in: Creep and Fracture in High Temperature Components - Design & Life Assessment Issues (2009), S. 1029 - 1037
[17]Quadakkers W.J. and Ennis P.J., Materials for Advanced Power Engineering 1998, Part I (1998) p. 123
[18]Nava-Paz J.C. and Knödler R., Materials for Advanced Power Engineering 1998, Part I (1998) p. 451
[19]Fukuda Y., Tamura K. and Sato T., Materials for Advanced Power Engineering 1998, Part I (1998) p. 461
[20]Ennis P.J. and Quadakkers W.J., Materials for Advanced Power Engineering 2002, Part II (2002) p. 1131
[21]Knödler R. and Scarlin B., Materials for Advanced Power Engineering 2002, Part III (2002) p. 1601
[22]Agüero A. and Muelas R., Materials Science Forum, 461-464 (2004) p. 957
[23]Zurek J., Nieto-Hierro L., Piron-Abellan J., Niewolak L., Singheiser L. and Quadakkers W.J., Materials Sceince Forum, 461-464 (2004) p. 791
[24]Lepingle V., Louis G., Petelot D., Lefevre B. and Vandenberghe B., Materials Science Forum, 461-464 (2004) p. 1039